

Orientational instabilities in nematic liquid crystals with weak anchoring under combined action of steady flow and external fields

I. Sh. Nasibullayev,^{1,2} O. S. Tarasov,³ A. P. Krekhov,^{1,3} and L. Kramer^{1,*}

¹*Physikalisches Institut, Universität Bayreuth, D-95440 Bayreuth, Germany*

²*Institute of Mechanics, Russian Academy of Sciences, 450054 Ufa, Russia*

³*Institute of Molecule and Crystal Physics, Russian Academy of Sciences, 450075 Ufa, Russia*

(Received 10 March 2005; revised manuscript received 9 September 2005; published 9 November 2005)

We study the homogeneous and the spatially periodic instabilities in a nematic liquid crystal layer subjected to steady plane *Couette* or *Poiseuille* flow. The initial director orientation is perpendicular to the flow plane. Weak anchoring at the confining plates and the influence of the external *electric* and/or *magnetic* field are taken into account. Approximate expressions for the critical shear rate are presented and compared with semianalytical solutions in case of *Couette* flow and numerical solutions of the full set of nematodynamic equations for *Poiseuille* flow. In particular the dependence of the type of instability and the threshold on the azimuthal and the polar anchoring strength and external fields is analyzed.

DOI: [10.1103/PhysRevE.72.051706](https://doi.org/10.1103/PhysRevE.72.051706)

PACS number(s): 61.30.Hn, 64.70.Md, 61.30.Cz

I. INTRODUCTION

Nematic liquid crystals (nematics) represent the simplest anisotropic fluid. The description of the dynamic behavior of the nematics is based on well established equations. The description is valid for low molecular weight materials as well as nematic polymers. The coupling between the preferred molecular orientation (director \mathbf{n}) and the velocity field leads to interesting flow phenomena in nematics. The orientational dynamics of nematics in flow strongly depends on the sign of the ratio of the Leslie viscosity coefficients $\lambda = \alpha_3 / \alpha_2$.

In typical low molecular weight nematics λ is positive (*flow-aligning materials*). The case of the initial director orientation perpendicular to the flow plane (spanned by the primary flow velocity and its gradient) has been clarified in classical experiments by Pieranski and Guyon [1,2] and theoretical works of Dubois-Violette and Manneville (for an overview see Ref. [3]). An additional external magnetic field could be applied along the initial director orientation. In *Couette* flow and low magnetic field there is a homogeneous instability [1]. For high magnetic field the homogeneous instability is replaced by a spatially periodic one leading to rolls [2]. In *Poiseuille* flow, as in *Couette* flow, the homogeneous instability is replaced by a spatially periodic one with increasing magnetic field [4]. All these instabilities are stationary.

Some nematics (in particular near a nematic-smectic transition) have negative λ (*non-flow-aligning materials*). For these materials in steady flow and in the geometry where the initial director orientation is perpendicular to the flow plane only spatially periodic instabilities are expected [5]. These materials demonstrate also tumbling motion [6] in the geometry where the initial director orientation is perpendicular to the confined plates that make the orientational behavior quite complicated.

Most previous theoretical investigations of the orientational dynamics of nematics in shear flow were carried out

under the assumption of strong anchoring of the nematic molecules at the confining plates. However, it is known that there is substantial influence of the boundary conditions on the dynamical properties of nematics in hydrodynamic flow [7–11]. Indeed, the anchoring strength strongly influences the orientational behavior and dynamic response of nematics under external electric and magnetic fields. This changes, for example, the switching times in bistable nematic cells [7], which play an important role in applications [12]. Recently the influence of the surface anchoring on the homogeneous instabilities in steady flow was investigated theoretically [9,11].

In this paper we study the combined action of steady flow (*Couette* and *Poiseuille*) and external fields (electric and magnetic) on the orientational instabilities of the nematics with initial orientation perpendicular to the flow plane. We focus on *flow-aligning* nematics. The external electric field is applied across the nematic layer and the external magnetic field is applied perpendicular to the flow plane. We analyze the influence of weak azimuthal and polar anchoring and of external fields on both homogeneous and spatially periodic instabilities.

In Sec. II the formulation of the problem based on the standard set of Ericksen-Leslie hydrodynamic equations [13] is presented. Boundary conditions and the critical Fréedericksz field in case of weak anchoring are discussed. In Sec. III equations for the homogeneous instabilities are presented. Rigorous semianalytical expressions for the critical shear rate for *Couette* flow (Sec. III A), the numerical scheme for finding threshold for *Poiseuille* flow (Sec. III B), and approximate analytical expressions for both types of flows (Sec. III C) are presented. In Sec. IV the analysis of the spatially periodic instabilities is given and in Sec. V we discuss the results. In particular we will be interested in the boundaries in parameter space (anchoring strengths, external fields) for the occurrence of the different types of instabilities.

*Deceased.

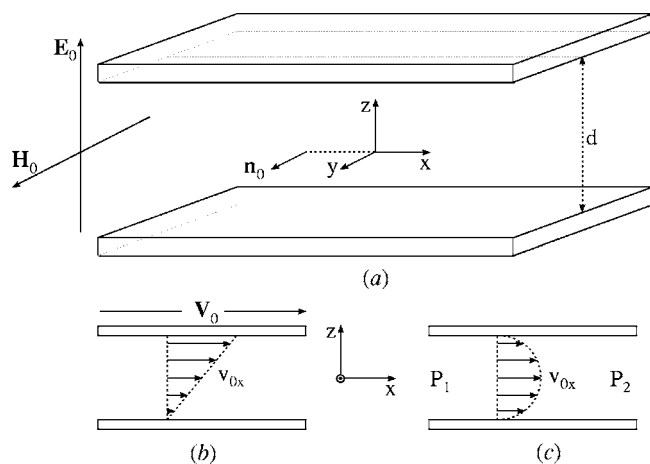


FIG. 1. Geometry of NLC cell (a). Couette (b) and Poiseuille (c) flows.

II. BASIC EQUATIONS

Consider a nematic layer of thickness d sandwiched between two infinite parallel plates that provide weak anchoring [Fig. 1(a)]. The origin of the Cartesian coordinates is placed in the middle of the layer with the z axis perpendicular to the confining plates ($z = \pm d/2$ for the upper or lower plate). The flow is applied along x . Steady Couette flow is induced by moving the upper plate with constant velocity V_0 [Fig. 1(b)]. Steady Poiseuille flow is induced by applying constant pressure difference $\Delta P = P_2 - P_1$ along x [Fig. 1(c)]. An external electric field \mathbf{E}_0 is applied along z and a magnetic field \mathbf{H}_0 along y .

The standard set of the nematodynamic equations [13] consists of the director equation

$$\gamma_1(\partial_t + \mathbf{v} \cdot \nabla)\mathbf{n} = \gamma_1\mathbf{\Omega} \times \mathbf{n} + \delta_{\perp}^{\perp}(-\gamma_2 A\mathbf{n} + \mathbf{h}), \quad (1)$$

where γ_1, γ_2 are rotational viscosities,

$$\gamma_1 = \alpha_3 - \alpha_2, \quad \gamma_2 = \alpha_6 - \alpha_5 = \alpha_3 + \alpha_2, \quad (2)$$

and Eqs. (5) and (7) below. Here α_k denote the Leslie viscosity coefficients and we have used the Parodi relation. In Eq. (1) $\mathbf{\Omega} = (\nabla \times \mathbf{v})/2$ is the local fluid rotation, $\delta_{ij}^{\perp} = \delta_{ij} - n_i n_j$ is the projection tensor which imposes the normalization of \mathbf{n} ($n^2 = 1$), $A_{ij} = (v_{i,j} + v_{j,i})/2$ is the hydrodynamic strain, and \mathbf{h} is the force on the director derived from the orientational free energy density

$$h_i = \frac{\partial}{\partial x_j} \frac{\partial F}{\partial n_{i,j}} - \frac{\partial F}{\partial n_i} \quad (3)$$

(j denotes the partial derivative with respect to the spatial coordinate x_j) where F is

$$F = \frac{1}{2} \{ K_{11}(\nabla \cdot \mathbf{n})^2 + K_{22}[\mathbf{n} \cdot (\nabla \times \mathbf{n})]^2 + K_{33}[\mathbf{n} \times (\nabla \times \mathbf{n})]^2 - \varepsilon_0 \varepsilon_a (\mathbf{n} \cdot \mathbf{E}_0)^2 - \mu_0 \chi_a (\mathbf{n} \cdot \mathbf{H}_0)^2 \}. \quad (4)$$

Here K_{ii} are the elastic constants, ε_a is the anisotropy of the dielectric permittivity, and χ_a is the anisotropy of the magnetic susceptibility.

The Navier-Stokes equation (momentum balance) has the form

$$\rho(\partial_t + \mathbf{v} \cdot \nabla)v_i = -p_{,i} + [T_{ji}^v + T_{ji}^e]_{,j}, \quad (5)$$

where ρ is the mass density of the NLC, p is the pressure, and the viscous and elastic parts of the stress tensor are

$$\begin{aligned} T_{ij}^v &= \alpha_1 n_i n_j A_{km} n_k n_m + \alpha_2 n_i N_j + \alpha_3 n_j N_i \\ &\quad + \alpha_4 A_{ij} + \alpha_5 n_i n_k A_{kj} + \alpha_6 n_j n_k A_{ki}, \\ T_{ij}^e &= -\frac{\partial F}{\partial n_{k,i}} n_{k,j}, \end{aligned} \quad (6)$$

where $N = (\partial_t + \mathbf{v} \cdot \nabla)\mathbf{n} - \mathbf{\Omega} \times \mathbf{n}$. In addition we have the incompressibility condition

$$\nabla \cdot \mathbf{v} = 0. \quad (7)$$

The basic state is given by the stationary homogeneous solution of Eqs. (1), (5), and (7):

$$\begin{aligned} \mathbf{n}_0 &= (0, 1, 0), \quad \mathbf{v}_0 = [v_{0x}(z), 0, 0], \\ p_0 &= \begin{cases} 0, & \text{for Couette flow,} \\ (\Delta P / \Delta x)x, & \text{for Poiseuille flow,} \end{cases} \end{aligned} \quad (8)$$

where for Couette flow

$$v_{0x} = V_0(1/2 + z/d), \quad (9)$$

and for Poiseuille flow

$$v_{0x} = -(\Delta P / \Delta x)(d^2 / \alpha_4)(1/4 - z^2/d^2). \quad (10)$$

In order to investigate the stability of the basic state (8) with respect to small perturbations we write

$$\begin{aligned} \mathbf{n} &= \mathbf{n}_0 + \mathbf{n}_1(z)e^{\sigma t} e^{iqy}, \quad \mathbf{v} = \mathbf{v}_0 + \mathbf{v}_1(z)e^{\sigma t} e^{iqy}, \\ p &= p_0 + p_1(z)e^{\sigma t} e^{iqy}. \end{aligned} \quad (11)$$

Guided by the experimental observations we assume that the wave vector of the destabilizing modes, if not zero, is perpendicular to the flow plane. The case $q=0$ corresponds to a homogeneous instability. Here we analyze stationary bifurcations, thus the threshold condition is $\sigma=0$.

It follows from the director normalization $n^2=1$ that $n_{1y} \equiv 0$ in linear approximation. The linearized equations (1), (5), and (7) are

$$(K_{22}\partial_z^2 - K_{33}q^2 - \mu_0\chi_a H_0^2)n_{1x} - \alpha_2 v_{0x,z}n_{1z} - iq\alpha_2 v_{1x} = 0, \quad (12)$$

$$\begin{aligned} (K_{11}\partial_z^2 - K_{33}q^2 + \varepsilon_0\varepsilon_a E_0^2 - \mu_0\chi_a H_0^2)n_{1z} - \alpha_3 v_{0x,z}n_{1x} - \alpha_3 \partial_z v_{1y} \\ - iq\alpha_2 v_{1z} = 0, \end{aligned} \quad (13)$$

$$-\rho v_{0x,z}v_{1z} + (\eta_3\partial_z^2 - \eta_1 q^2)v_{1x} + iq(\eta_1 - \eta_3)v_{0x,z}n_{1z} = 0, \quad (14)$$

$$\begin{aligned} -iqp_1 + [\eta_2\partial_z^2 - (\eta_4 - \eta_3 - \eta_5)q^2]v_{1y} \\ - (\eta_3 - \eta_2)\partial_z(v_{0x,z}n_{1x}) = 0, \end{aligned} \quad (15)$$

$$-\partial_z p_1 + [(\eta_3 + \eta_5)\partial_z^2 - \eta_1 q^2]v_{1z} - iq\eta_5 v_{0xz} n_{1x} = 0, \quad (16)$$

$$iqv_{1y} + \partial_z v_{1z} = 0, \quad (17)$$

where $\eta_1 = (\alpha_4 + \alpha_5 - \alpha_2)/2$, $\eta_2 = (\alpha_3 + \alpha_4 + \alpha_6)/2$, $\eta_3 = \alpha_4/2$, $\eta_4 = \alpha_1 + \eta_1 + \eta_2$, $\eta_5 = -(\alpha_2 + \alpha_5)/2$.

The anchoring properties of the director are characterized by a surface energy per unit area F_s , which has a minimum when the director at the surface is oriented along the *easy axis* (parallel to the y axis in our case). A phenomenological expression for the surface energy F_s can be written in terms of an expansion with respect to $(\mathbf{n} - \mathbf{n}_0)$. For small director deviations from the easy axis one obtains

$$F_s = \frac{1}{2}W_a n_{1x}^2 + \frac{1}{2}W_p n_{1z}^2, \quad W_a > 0, \quad W_p > 0, \quad (18)$$

where W_a and W_p are the ‘‘azimuthal’’ and ‘‘polar’’ anchoring strengths, respectively. W_a characterizes the surface energy increase due to distortions within the substrate plane and W_p relates to distortions out of the substrate plane. The boundary conditions for the director perturbations can be obtained from the surface torques balance equation

$$\pm \frac{\partial F}{\partial n_{1i,z}} + \frac{\partial F_s}{\partial n_{1i}} = 0, \quad (19)$$

with ‘‘ \pm ’’ for $z = \pm d/2$ and $i = x, z$. Taking into account Eq. (18) the boundary conditions for the director perturbations (19) can be written as

$$\pm K_{22} n_{1x,z} + W_a n_{1x} = 0, \quad \pm K_{11} n_{1z,z} + W_p n_{1z} = 0, \quad (20)$$

with ‘‘ \pm ’’ for $z = \pm d/2$. It is convenient to introduce dimensionless parameters as ratios of the characteristic anchoring length (K_{ii}/W_i) over the layer thickness d ,

$$\beta_a = K_{22}/(W_a d), \quad \beta_p = K_{11}/(W_p d). \quad (21)$$

In the limit of strong anchoring, $(\beta_a, \beta_p) \rightarrow 0$, one has $n_{1x} = n_{1z} = 0$ at $z = \pm d/2$. For torque-free boundary conditions, $(\beta_a, \beta_p) \rightarrow \infty$, one has $n_{1x,z} = n_{1z,z} = 0$ at the boundaries. From Eq. (21) one can see that by changing the thickness d , the dimensionless parameters β_a and β_p can be varied with the ratio β_a/β_p remaining constant.

The boundary conditions for the velocity perturbations (no-slip) are

$$v_{1x}(z = \pm d/2) = 0, \quad (22)$$

$$v_{1y}(z = \pm d/2) = 0, \quad (23)$$

$$v_{1z}(z = \pm d/2) = v_{1z,z}(z = \pm d/2) = 0. \quad (24)$$

The symmetry properties of the solutions of Eqs. (12)–(17) under the reflection $z \rightarrow -z$ is shown in Table I. We will always classify the solutions by the z symmetry of the x component of the director perturbation n_{1x} (first row in Table I).

In the case of positive ε_a , for some critical value of the electric field the basic state loses its stability already in the

TABLE I. Symmetry properties of the solutions of Eqs. (12)–(17) under $\{z \rightarrow -z\}$.

Perturbation	Couette flow		Poiseuille flow	
	‘‘odd’’	‘‘even’’	‘‘odd’’	‘‘even’’
n_{1x}	odd	even	odd	even
n_{1z}	odd	even	even	odd
v_{1x}	odd	even	odd	even
v_{1y}	even	odd	odd	even
v_{1z}	odd	even	even	odd
p_1	even	odd	odd	even

absence of flow (*Fréedericksz transition*). Clearly the Fréedericksz transition field depends on the polar anchoring strength W_p . There is competition of the elastic torque ($K_{11}\partial_z^2 n_{1z}$) and the field-induced torque ($\varepsilon_0 \varepsilon_a E_0^2 n_{1z}$). The solution of Eq. (13) with $n_{1x} = 0$, $v_{1y} = 0$, $q = 0$, and $H_0 = 0$ has the form

$$n_{1z} = C \cos(\pi \delta z/d), \quad \delta = E_F^{weak}/E_F, \quad (25)$$

where E_F^{weak} is the actual Fréedericksz transition field and $E_F = (\pi/d)\sqrt{K_{11}/(\varepsilon_0 \varepsilon_a)}$ is the critical Fréedericksz field for strong anchoring. After substituting n_{1z} into the boundary conditions (20) we obtain the expression for δ ,

$$\tan(\pi \delta/2) = 1/(\pi \delta \beta_p). \quad (26)$$

One easily sees that $\delta \rightarrow 1$ for $\beta_p \rightarrow 0$ and $\delta \rightarrow \sqrt{2/\beta_p}/\pi$ for $\beta_p \rightarrow \infty$. For $\beta_p = 1$ one gets $E_F^{weak} = 0.42 E_F$.

III. HOMOGENEOUS INSTABILITY

In the case of homogeneous perturbations ($q = 0$) from Eqs. (14), (16), and (17) and boundary conditions (22)–(24) we deduce $v_{1x} = 0$, $v_{1z} = 0$, and $p_1 = 0$. In order to simplify equations for n_{1x} , n_{1z} , and v_{1y} we use dimensionless variables as in Ref. [9]

$$\tilde{z} = z/d, \quad \tilde{q} = qd,$$

$$N_{1x} = \beta n_{1x}, \quad N_{1z} = n_{1z}, \quad V_{1y} = \beta^2 \eta_{23} \frac{\tau_d}{d} v_{1y},$$

$$\tilde{S} = \beta \tau_d v_{0xz}, \quad \beta^2 = \alpha_{32} k_{21} \eta_{32}, \quad \tau_d = \frac{(-\alpha_2) d^2}{K_{22}}, \quad (27)$$

where $\eta_{ij} = \eta_i/\eta_j$, $\alpha_{ij} = \alpha_i/\alpha_j$, $k_{ij} = K_{ii}/K_{jj}$. This leads to the following equations (tildes are omitted)

$$(\partial_z^2 - h)N_{1x} + SN_{1z} = 0, \quad (28)$$

$$(\partial_z^2 + e - k_{21}h)N_{1z} + \eta_{23}SN_{1x} + \partial_z V_{1y} = 0, \quad (29)$$

$$\partial_z^2 V_{1y} - (1 - \eta_{23})\partial_z(SN_{1x}) = 0, \quad (30)$$

where $h = \pi^2 H_0^2/H_F^2$, $e = \text{sgn}(\varepsilon_a)\pi^2 E_0^2/E_F^2$, and $H_F = (\pi/d)\sqrt{K_{22}/(\mu_0 \chi_a)}$, $E_F = (\pi/d)\sqrt{K_{11}/(\varepsilon_0 \varepsilon_a)}$ are the critical

Fréedericksz transition fields for strong anchoring. For the shear rate S one has, for Couette flow,

$$S = a^2, \quad a^2 = \frac{V_0 \tau_d}{d} \beta \quad (31)$$

and for Poiseuille flow,

$$S = -a^2 z, \quad a^2 = -\frac{\Delta P}{\Delta x} \frac{\tau_d d}{\eta_3} \beta. \quad (32)$$

The boundary conditions (20) and (23) reduced to

$$\pm \beta_a N_{1x,z} + N_{1x} = 0, \quad \pm \beta_p N_{1z,z} + N_{1z} = 0, \quad \text{for } z = \pm 1/2, \quad (33)$$

$$V_{1y}(z = \pm 1/2) = 0. \quad (34)$$

A. Couette flow

For Couette flow the solution of Eqs. (28)–(30) can be obtained semianalytically. For the “odd” solution one gets

$$N_{1x} = C_1 \sinh(\xi_1 z) + C_2 \sin(\xi_2 z),$$

$$N_{1z} = C_3 \sinh(\xi_1 z) + C_4 \sin(\xi_2 z),$$

$$V_{1y} = C_5 \cosh(\xi_1 z) + C_6 \cos(\xi_2 z) + C_7. \quad (35)$$

Taking into account the boundary conditions (33) and (34) the solvability condition for the C_i (“boundary determinant” equal to zero) gives an expression for the critical shear rate a_c^2 , at which the basic state (8) loses its stability,

$$(h + \xi_2^2) \left[\beta_a \xi_1 + \tanh\left(\frac{\xi_1}{2}\right) \right] \left[\beta_p \xi_2 + \tan\left(\frac{\xi_2}{2}\right) \right] - (h - \xi_1^2) \times \left[\beta_a \xi_2 + \tan\left(\frac{\xi_2}{2}\right) \right] \left[\beta_p \xi_1 + \tanh\left(\frac{\xi_1}{2}\right) \right] = 0, \quad (36)$$

where

$$\xi_1^2 = \frac{b + \sqrt{c^2 + 4a_c^4}}{2}, \quad \xi_2^2 = \frac{-b + \sqrt{c^2 + 4a_c^4}}{2},$$

$$b = (1 + k_{21})h - e, \quad c = (1 - k_{21})h + e. \quad (37)$$

For the “even” solution one obtains

$$N_{1x} = C_1 \cosh(\xi_1 z) + C_2 \cos(\xi_2 z) + C_3,$$

$$N_{1z} = C_4 \cosh(\xi_1 z) + C_5 \cos(\xi_2 z) + C_6,$$

$$V_{1y} = C_7 \sinh(\xi_1 z) + C_8 \sin(\xi_2 z) + C_9 z. \quad (38)$$

The boundary conditions (33) and (34) now lead to the following condition (“boundary determinant”):

$$\begin{vmatrix} 1 & h & \frac{h(k_{21}h-e) - \eta_{23}a_c^4}{2a_c^4(1-\eta_{23})} \\ -\beta_a \xi_2 \tan(\xi_2/2) + 1 & (h + \xi_2^2)[- \beta_p \xi_2 \tan(\xi_2/2) + 1] & \frac{\tan(\xi_2/2)}{\xi_2} \\ \beta_a \xi_1 \tanh(\xi_1/2) + 1 & (h - \xi_1^2)[\beta_p \xi_1 \tanh(\xi_1/2) + 1] & \frac{\tanh(\xi_1/2)}{\xi_1} \end{vmatrix} = 0, \quad (39)$$

where ξ_1, ξ_2 are defined in Eq. (37). Expressions (36) and (39) allow us to determine the influence of anchoring conditions (β_a, β_p) and external fields on the critical shear rate a_c^2 .

B. Poiseuille flow

In the case of Poiseuille flow the system (28)–(30) with $S = -a^2 z$ admits an analytical solution only in the absence of external fields (in terms of Airy functions) [9]. In the presence of fields we solve the problem numerically. In the framework of the Galerkin method we expand N_{1x}, N_{1z} , and V_{1y} in a series,

$$N_{1x} = \sum_{n=1}^{\infty} C_{1,n} f_n(z), \quad N_{1z} = \sum_{n=1}^{\infty} C_{2,n} g_n(z),$$

$$V_{1y} = \sum_{n=1}^{\infty} C_{3,n} u_n(z), \quad (40)$$

where the trial functions f_n, g_n , and u_n satisfy the boundary conditions (33) and (34). For the “odd” solution we write

$$f_n(z) = \zeta_n^o(z; \beta_a), \quad g_n(z) = \zeta_n^e(z; \beta_p), \quad u_n(z) = \nu_n^o(z), \quad (41)$$

and for the “even” solution

$$f_n(z) = \zeta_n^e(z; \beta_a), \quad g_n(z) = \zeta_n^o(z; \beta_p), \quad u_n(z) = \nu_n^e(z). \quad (42)$$

The functions $\zeta_n^o(z; \beta), \zeta_n^e(z; \beta), \nu_n^o(z)$, and $\nu_n^e(z)$ are given in Appendix I. In our calculations we have to truncate the expansions (40) to a finite number of modes.

TABLE II. Trial functions for the homogeneous solutions.

Function	Couette flow		Poiseuille flow	
	“odd”	“even”	“odd”	“even”
$f(z)$	$\xi_1^o(z; \beta_a)$	$\xi_1^e(z; \beta_a)$	$\xi_1^o(z; \beta_a)$	$\xi_1^e(z; \beta_a)$
$g(z)$	$\xi_1^o(z; \beta_p)$	$\xi_1^e(z; \beta_p)$	$\xi_1^o(z; \beta_p)$	$\xi_1^e(z; \beta_p)$

After substituting Eq. (40) into the system (28)–(30) and projecting the equations on the trial functions $f_n(z), g_n(z)$, and $u_n(z)$ one gets a system of linear homogeneous algebraic equations for $\mathbf{X} = \{C_{i,n}\}$ in the form $(A - a^2 B)\mathbf{X} = 0$. We have solved this eigenvalue problem for a^2 . The lowest (real) eigenvalue corresponds to the critical shear rate a_c^2 . According to the two types of z symmetry of the solutions (and of the set of trial functions) one obtains the threshold values of a_c^2 for the “odd” and “even” instability modes. The number of Galerkin modes was chosen such that the accuracy of the calculated eigenvalues was better than 1% (we took ten modes in case of “odd” solution and five modes for “even” solution).

C. Approximate analytical expression for the critical shear rate

In order to obtain an *easy-to-use* analytical expression for the critical shear rate as a function of the surface anchoring strengths and the external fields we use the lowest-mode approximation in the framework of the Galerkin method. By integrating Eq. (30) over z one can eliminate $\partial_z V_{1y}$ from Eq. (29) which gives

$$(\partial_z^2 + e - k_{21}h)N_{1z} + SN_{1x} = K, \quad (43)$$

where K is an integration constant. Taking into account the boundary conditions for V_{1y} one has

$$K = (1 - \eta_{23}) \int_{-1/2}^{1/2} (SN_{1x}) dz. \quad (44)$$

We choose for the director components N_{1x}, N_{1z} the one-mode approximation

$$N_{1x} = C_1 f(z), \quad N_{1z} = C_2 g(z), \quad (45)$$

where $f(z)$ and $g(z)$ are given in Table II and Appendix I. Substituting Eq. (45) into Eqs. (28) and (43) and projecting the first equation on $f(z)$ and the second one on $g(z)$ we get algebraic equations for C_i . The solvability condition gives the expression for the critical shear rate

$$a_c^2 = \sqrt{c_1 c_2 / c_3}, \quad (46)$$

with

$$c_1 = \langle f f'' \rangle - h \langle f^2 \rangle,$$

$$c_2 = \langle g g'' \rangle + (e - k_{21}h) \langle g^2 \rangle,$$

$$c_3 = \langle f s g \rangle [\langle f s g \rangle - (1 - \eta_{23}) \langle g \rangle \langle s f \rangle], \quad (47)$$

where $\langle \dots \rangle$ denotes a spatial average (projection integral)

$$\langle \dots \rangle = \int_{-1/2}^{1/2} (\dots) dz. \quad (48)$$

The values for the integrals $\langle \dots \rangle$ are given in Appendix II. Expression (46) can be used for both Couette and Poiseuille flow by choosing the function $s(z)$ [for Couette flow $s(z) = 1$ and for Poiseuille flow $s(z) = -z$] and the trial functions $f(z)$ and $g(z)$ with appropriate symmetry.

In comparison with the rigorous calculations for the material parameters of MBBA at 25 °C [14] in the case of Couette flow the one-mode approximation (46) for the “odd” solution has an accuracy that varies from 2.5% to 16% when H_0/H_F varies from 0 to 4. The “even” solution has the accuracy of 1–8% for $0 \leq H_0/H_F \leq 3$ and of 1–12% for $0 \leq E_0/E_F \leq 0.6$.

For Poiseuille flow for odd solution the accuracy is 30% in the absence of fields. For the even solution the accuracy is 12–15% for magnetic fields $0 \leq H_0/H_F \leq 0.5$.

For both Couette and Poiseuille flow the accuracy of the formula (46) decreases with increasing field strengths.

IV. SPATIALLY PERIODIC INSTABILITY

For spatially periodic perturbations ($q \neq 0$) eliminating v_{1y} from Eq. (13) by use of the incompressibility condition (17) and the pressure p_1 by taking z derivative of Eq. (15) one obtains the equations for n_{1x}, n_{1z}, v_{1x} , and v_{1z} . We used again the renormalized variables (27) with

$$V_{1x} = \beta \frac{\tau_d}{d} v_{1x}, \quad V_{1z} = \beta^2 \eta_{23} \frac{\tau_d}{d} v_{1z}, \quad (49)$$

which gives

$$(\partial_z^2 - k_{32}q^2 - h)N_{1x} + SN_{1z} + iqV_{1x} = 0, \quad (50)$$

$$iq(\partial_z^2 - k_{31}q^2 + e - k_{21}h)N_{1z} + iq\eta_{23}SN_{1x} - (\partial_z^2 + \alpha_{23}q^2)V_{1z} = 0, \quad (51)$$

$$- \frac{\tau_v}{\tau_d} (\beta^2 \eta_{23})^{-1} S V_{1z} + (\partial_z^2 - \eta_{13}q^2)V_{1x} + iq(\eta_{13} - 1)SN_{1z} = 0, \quad (52)$$

$$(\partial_z^4 - \eta_{42}q^2 \partial_z^2 + \eta_{12}q^4)V_{1z} + iq[(1 - \eta_{23})\partial_z^2 + \eta_{53}q^2](SN_{1x}) = 0, \quad (53)$$

and dimensionless shear rate S is defined by Eqs. (31) and (32). The convective term in Eq. (52) is proportional to the ratio of the viscous relaxation time $\tau_v = \rho d^2 / \eta_3$ to the director relaxation time $\tau_d = (-\alpha_2) d^2 / K_{22}$ and can therefore safely be neglected since for the typical NLC material parameters [$\rho \sim 10^3$ kg/m³, $\eta_3 \sim (-\alpha_2) \sim 10^{-1}$ Pa·s, $K_{22} \sim 10^{-11}$ N] one has $\tau_v / \tau_d \sim 10^{-6}$.

We have the boundary conditions for the director (33) and for the velocity

$$V_{1x}(z = \pm 1/2) = 0,$$

$$V_{1z}(z = \pm 1/2) = V_{1z,z}(z = \pm 1/2) = 0. \quad (54)$$

TABLE III. Trial functions for the spatially periodic solutions.

Function	Couette flow		Poiseuille flow	
	“odd”	“even”	“odd”	“even”
$f_n(z)$	$\zeta_n^o(z; \beta_a)$	$\zeta_n^e(z; \beta_a)$	$\zeta_n^o(z; \beta_a)$	$\zeta_n^e(z; \beta_a)$
$g_n(z)$	$\zeta_n^o(z; \beta_p)$	$\zeta_n^e(z; \beta_p)$	$\zeta_n^o(z; \beta_p)$	$\zeta_n^e(z; \beta_p)$
$u_n(z)$	$\nu_n^o(z)$	$\nu_n^e(z)$	$\nu_n^o(z)$	$\nu_n^e(z)$
$w_n(z)$	$s_n^o(z)$	$s_n^e(z)$	$s_n^o(z)$	$s_n^e(z)$

The system (50)–(53) with boundary conditions (33) and (54) has no analytical solution. Thus we solved the problem numerically in the framework of the Galerkin method

$$N_{1x} = \sum_{n=1}^{\infty} C_{1,n} f_n(z), \quad N_{1z} = \sum_{n=1}^{\infty} C_{2,n} g_n(z),$$

$$V_{1x} = \sum_{n=1}^{\infty} C_{3,n} u_n(z), \quad V_{1z} = \sum_{n=1}^{\infty} C_{4,n} w_n(z), \quad (55)$$

where the trial functions f_n, g_n, u_n , and w_n satisfy the boundary conditions (33) and (54) (see Table III and Appendix I). After substituting Eq. (55) into the system (50)–(53) and projecting onto corresponding trial functions $f_n(z), g_n(z), u_n(z), w_n(z)$ we get a system of linear homogeneous algebraic equations for $X = \{C_{i,n}\}$. This system has the form $[A(q) - a^2(q)B(q)]X = 0$. Truncating the expansion (55) we have solved the eigenvalue problem numerically to find the neutral curve $a_0^2(q)$. The minimum of $a_0^2(q)$ yields the critical wave number $q = q_c$ and the critical shear rate $a_c^2 = a_0^2(q_c)$. The number of Galerkin modes was chosen such that the accuracy of the calculated a_c^2 and q_c was better than 1% (ten modes for odd solution and five modes for even solution).

In order to get an approximate expression for the threshold we use the lowest-mode approximation in the framework of the Galerkin method. We used the same scheme described above for the single mode [$n=1$ in expansion (55)] and get the following formula for the critical shear rate

$$a_c^2 = \sqrt{m_1 m_2 / (m_3 m_4)}, \quad (56)$$

with

$$m_1 = \langle ff'' \rangle - (k_{32} q^2 + h) \langle f^2 \rangle,$$

$$m_2 = \langle gg'' \rangle - (k_{31} q^2 - e + k_{21} h) \langle g^2 \rangle,$$

$$m_3 = \langle fs g \rangle + (\eta_{13} - 1) q^2 \langle us g \rangle \langle fu \rangle / r_1,$$

$$m_4 = \langle fs g \rangle + [\langle gw'' \rangle + \alpha_{23} q^2 \langle gw \rangle] \\ \times [(1 - \eta_{23}) \langle w [sf]'' \rangle + \eta_{53} q^2 \langle wsf \rangle] / r_2,$$

$$r_1 = \langle uu'' \rangle - \eta_{13} q^2 \langle u^2 \rangle,$$

$$r_2 = \langle ww^{(4)} \rangle - \eta_{42} q^2 \langle ww'' \rangle + \eta_{12} q^4 \langle w^2 \rangle. \quad (57)$$

The values of the projection integrals $\langle \dots \rangle$ are given in Appendix II. Expression (56) can be used for both Couette and Poiseuille flow by choosing the function $s(z)$ [for Couette flow $s(z)=1$ and for Poiseuille flow $s(z)=-z$] and the trial functions f, g, u , and w with appropriate symmetry. Minimization of Eq. (56) with respect to q gives the critical wave number q_c .

In the case of Couette flow and strong anchoring an approximate analytical expression for a_c^2 was obtained in Ref. [15] using trial functions that satisfy free-slip boundary conditions for the velocity. The formula (56) is more accurate because we chose for V_{1z} Chandrasekhar functions that satisfy the boundary conditions (54).

For the calculations we used material parameters of MBBA at 25 °C [14]. Compared with the rigorous calculations the accuracy of Eq. (56) is better than 1% for Couette flow and better than 3% for Poiseuille flow. Note that Eq. (46) for the homogeneous instability is more accurate than Eq. (56) for $q=0$ because Eq. (56) was obtained by solving four equations (50)–(53) by approximating all variables, whereas Eq. (46) was obtained by solving the reduced equations (28) and (43) by approximating only two variables.

V. RESULTS AND DISCUSSION

For the calculations we used material parameters of MBBA at 25 °C [14]. Calculations were made for the range of anchoring lengths $\beta_a=0-1$ and $\beta_p=0-1$. For strong anchoring $\beta_a=\beta_p=0$, whereas $\beta_a=\beta_p=1$ correspond to very weak anchoring when the characteristic anchoring lengths are equal to the NLC layer thickness.

A. Couette flow

We found that in the case of Couette flow without and with an additional electric field the critical shear rate a_c^2 for the even type homogeneous instability (EH) is systematically lower than the threshold for other types of instability. Note that in the presence of the field the symmetry with respect to the exchange $\beta_a \leftrightarrow \beta_p$ is broken.

In Fig. 2 contour plots for the critical shear rate a_c^2 vs anchoring lengths β_a and β_p for different values of the electric field are shown. The difference between a_c^2 obtained from the exact, semianalytical solution (39) and from the one-mode approximation (46) is indistinguishable in the figure.

In Fig. 3 contour plots of a_c^2 (thin dashed lines) and the boundaries where the type of instability changes [the thick solid lines are obtained numerically, the thick dashed lines are from Eqs. (46) and (56)] are shown for different values of magnetic field. For not too strong magnetic field in the region of weak anchoring the odd type homogeneous instability (OH) takes place [Fig. 3(a)]. In the region of strong anchoring, $(\beta_a, \beta_p) \rightarrow 0$, one has homogeneous instability of opposite z symmetry (EH). Note that the threshold for the EH instability becomes less sensitive to the surface anchoring [Fig. 3(a)]. Increasing the magnetic field the OH region

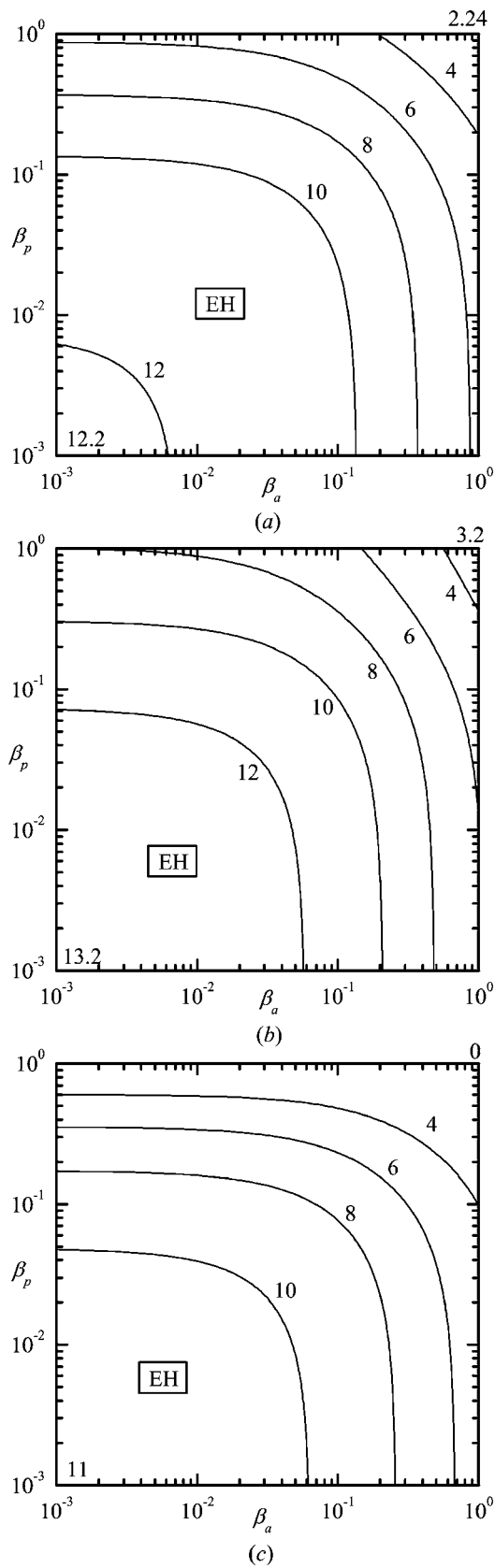


FIG. 2. Contour plot of the critical shear rate α_c^2 vs β_a and β_p for Couette flow. (a) $E_0=0$; (b) $E_0=E_F^{weak}$, $\epsilon_a < 0$; (c) $E_0=E_F^{weak}$, $\epsilon_a > 0$. $E_F^{weak}=0.42E_F$.

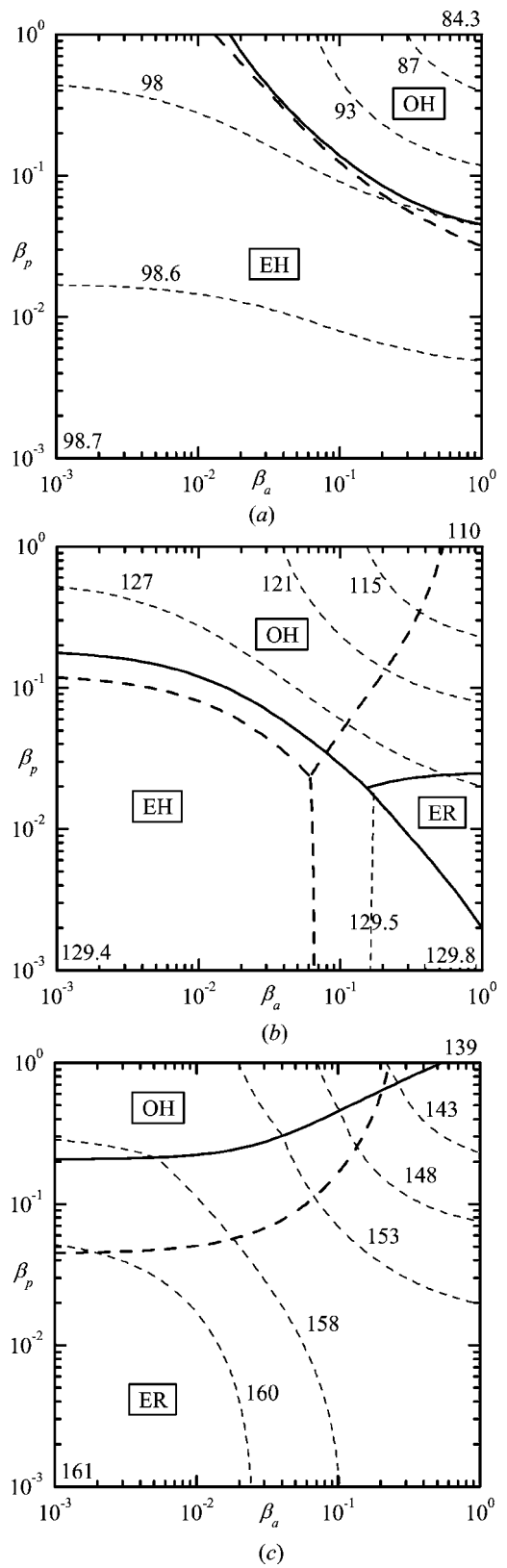


FIG. 3. Contour plot of the critical shear rate α_c^2 vs β_a and β_p for Couette flow with additional magnetic field. (a) $H_0/H_F=3$; (b) $H_0/H_F=3.5$; (c) $H_0/H_F=4$. Boundaries between different type of instabilities are given by thick solid lines (full numerical) and thick dashed lines (one-mode approximation).

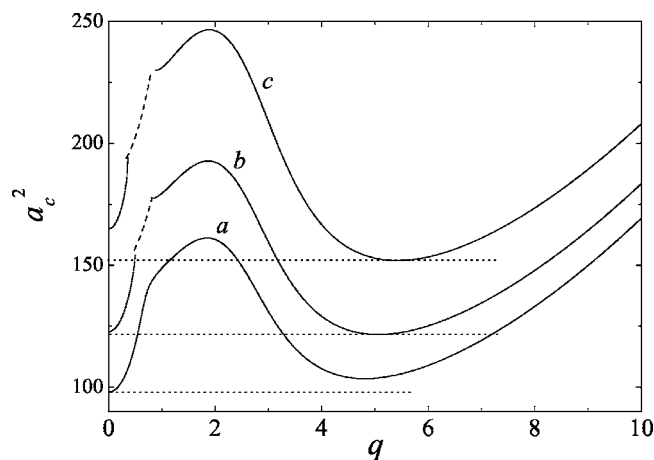


FIG. 4. Neutral curves a_c^2 vs q for Couette flow with additional magnetic field, $\beta_a=0.1$, $\beta_p=0.1$. (a) $H_0/H_F=3$; (b) $H_0/H_F=3.4$; (c) $H_0/H_F=4$.

expands toward stronger anchoring strengths. Above $H_0 \approx 3.2$ a region with lowest threshold corresponding to the even roll mode (ER) appears. This region has borders with both types of the homogeneous instability [Fig. 3(b)]. With further increasing magnetic field the region of spatially periodic instability ER expands [Fig. 3(c)] and above $H_0/H_F=4$ the ER instability has invaded the whole investigated range of (β_a, β_p) . For strong anchoring and $H_0/H_F=3.5$ the critical wave number of ER instability is $q_c=5.5$. It increases with increasing magnetic field and decreases with decreasing anchoring strengths.

Leslie has pointed out (using an approximate analytical approach) that for strong anchoring a transition from a homogeneous instability without transverse flow (EH) to one with such flow (OH) as the magnetic field is increased is not possible in MBBA because of the appearance of the ER type instability [16]. This is consistent with our results. We find that the EH-OH transition in MBBA is possible only in the region of weak anchoring [Figs. 3(a)–3(c)].

In Fig. 4 neutral curves for different values of the magnetic field and fixed anchoring lengths are shown (solid line for ER and dashed lines for OR). There are always two minima for the even mode; one of them at $q=0$ that corresponds to the homogeneous instability EH. For small magnetic field the absolute minimum is at $q=0$ (line a). The neutral curve for the odd mode OR is systematically higher than for ER. With increasing magnetic field the critical amplitude for the EH instability ($q=0$) increases more rapidly than the one for the ER instability ($q \neq 0$) so that for $H_0/H_F > 3.4$ the ER solution is realized (lines b and c). In a small range of q (dashed lines) a stationary ER solution does not exist but we have OR instead.

For the EH instability under Couette flow and strong anchoring in the absence of fields we find $a_c^2=12.15$ [from the semianalytical expression (39) as well as from the one-mode approximation (46) and also Eq. (56) with $q=0$]. The available experimental value for the critical shear velocity in MBBA at 23 °C is $V_{0c}=11.5 \mu\text{m/s}$ for a sample of thickness 200 μm [1], that gives $a_c^2=6.3$ for the material parameters [14]. We suspect that the lower experimental value is due to

failure of the strong anchoring limit and deviations of the initial director orientation from the direction perpendicular to the flow plane. In addition, the difference in the material parameters of the substance used in the experiment and that of “standard” MBBA can also lead to the discrepancy.

B. Poiseuille flow

In Fig. 5 the contour plot for a_c^2 [thin dashed lines are from the full numerical calculation, dotted lines are from the one-mode approximations (46) and (56)] and the boundaries for different types of instabilities [thick solid line: numerical; thick dashed line: Eqs. (46) and (56)] are shown. In Poiseuille flow the phase diagram is already very rich in the absence of external fields. In the region of large β_a (weak azimuthal anchoring) one has the EH instability. For intermediate anchoring strengths rolls of type OR occur [Fig. 5(a)]. Note that even in the absence of the fields there is no symmetry under exchange $\beta_a \leftrightarrow \beta_p$, contrary to Couette flow. The one-mode approximations (46) and (56) do not give the transition to EH for strong anchoring. From the full numerical calculations follows that in the region of strong anchoring, $(\beta_a, \beta_p) \rightarrow 0$, the difference between the EH and the OR instability thresholds is only about 5%. By varying material parameters (increase α_2 by 10% or decrease α_3 by 20% or α_5 by 25% or K_{33} by 35%) it is possible to change the type of instability in this region.

Application of an electric field leads for $\varepsilon_a < 0$ ($\varepsilon_a > 0$) to expansion (contraction) of the EH region [Figs. 5(b) and 5(c)]. At $E_0/E_F=1$ and $\varepsilon_a < 0$ rolls vanish completely and the EH instability occurs in the whole investigated area of (β_a, β_p) . For $\varepsilon_a > 0$ the instability of OH type appears in the region of large β_p (weak polar anchoring). In this case, increasing the electric field from E_F^{weak} to E_F causes an expansion of the OH region. Note that for $\beta_p > 1$, which is in the OH region, the Fréedericksz transition occurs first.

An additional magnetic field suppresses the homogeneous instability (Fig. 6). Above $H_0/H_F \approx 0.5$ the spatially periodic instability OR occurs for all anchoring strengths investigated.

The critical wave number q_c in the absence of fields is 1.4. Application of an electric field decreases q_c whereas the magnetic field increases q_c . The wave number decreases with decreasing anchoring strengths.

In the absence of fields and strong anchoring we find for the EH instability $a_c^2=102$ [Eq. (46) gives 110 and Eq. (56) with $q=0$ gives 130]. The experimental value for the critical pressure gradient in MBBA is $\Delta P_c/\Delta x=245 \text{ Pa/m}$ for a sample of thickness 200 μm [17,18], that gives $a_c^2=130$ for the material parameters [14]. Thus theoretical calculations and experimental results are in good agreement. Note that in the experiments [17,18] actually not steady but oscillatory flow with very low frequency was used ($f=5 \times 10^{-3} \text{ Hz}$).

In summary, the orientational instabilities for both steady Couette (semianalytical for homogeneous instability and numerical for rolls) and Poiseuille flow (numerical) were analyzed rigorously taking into account weak anchoring conditions at the confining plates and the influence of external fields. Easy-to-use expressions for the threshold of all pos-

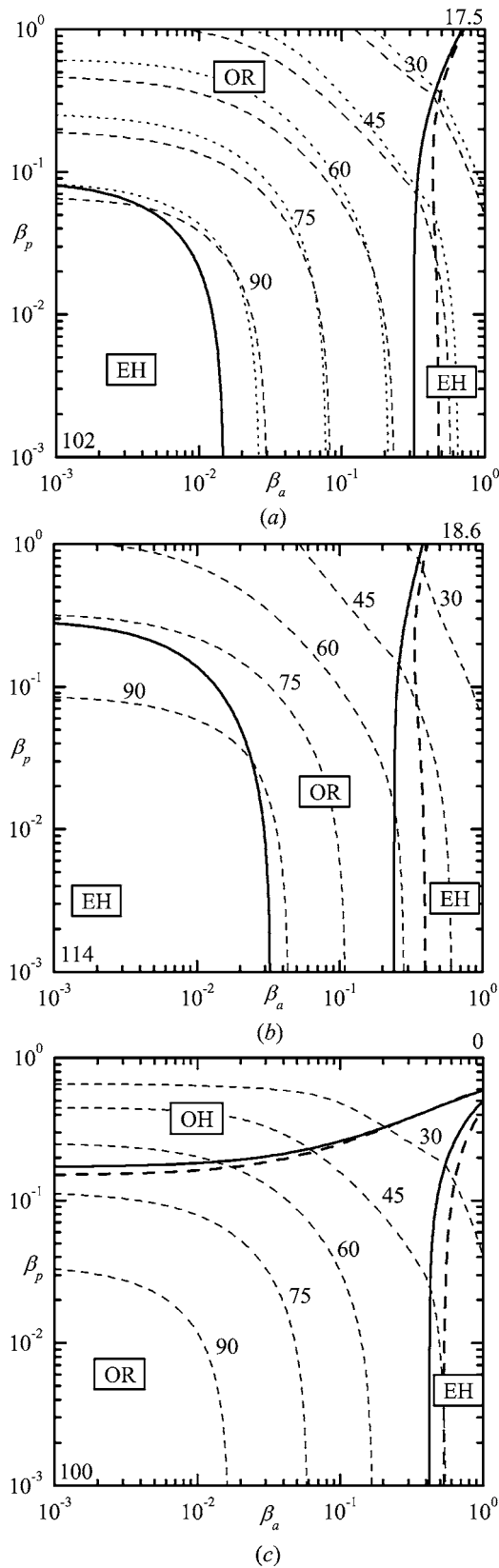


FIG. 5. Contour plot of the critical shear rate a_c^2 vs β_a and β_p for Poiseuille flow. (a) $E_0=0$; (b) $E_0=E_0^{weak}$, $\varepsilon_a < 0$; (c) $E_0=E_0^{weak}$, $\varepsilon_a > 0$. $E_F^{weak}=0.42E_F$. Boundaries between different types of instabilities are given by thick solid lines (full numerical) and thick dashed lines (one-mode approximation).

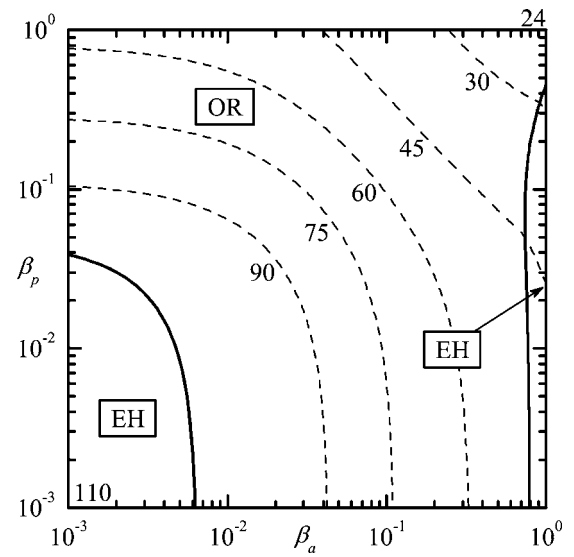


FIG. 6. Contour plot of the critical shear rate a_c^2 vs β_a and β_p for Poiseuille flow with additional magnetic field $H_0/H_F=0.4$.

sible types of instabilities were obtained and compared with the rigorous calculations. In particular the regions in parameter space (anchoring strengths, external fields) where the different types of instabilities occurred were determined. The results can be used for the experimental measurements of the polar and azimuthal anchoring strengths in one single experiment.

ACKNOWLEDGMENTS

We wish to thank W. Pesch for helpful discussions and critical reading of the manuscript. Financial support by DFG (EGK “Non-equilibrium phenomena and phase transition in complex systems” and Grant Nos. Kr690/14-1 and Kr690/22-1) and RFBR (Grant Nos. 05-02-16716, 05-02-16548, 05-02-97907) are gratefully acknowledged.

APPENDIX A: TRIAL FUNCTIONS

In the calculations we used the following set of trial functions for the director perturbations:

$$\zeta_n^o(z; \beta) = \sin(2n\pi z) + 2n\pi\beta \sin([2n-1]\pi z),$$

$$\zeta_n^e(z; \beta) = \cos([2n-1]\pi z) + (2n-1)\pi\beta \cos(2[n-1]\pi z),$$

and for the velocity perturbations

$$v_n^o(z) = \sin(2n\pi z), v_n^e(z) = \cos([2n-1]\pi z),$$

$$s_n^o(z) = \frac{\sinh(\lambda_{2n}z)}{\sinh(\lambda_{2n}/2)} - \frac{\sin(\lambda_{2n}z)}{\sin(\lambda_{2n}/2)},$$

$$s_n^e(z) = \frac{\cosh(\lambda_{2n-1}z)}{\cosh(\lambda_{2n-1}/2)} - \frac{\cos(\lambda_{2n-1}z)}{\cos(\lambda_{2n-1}/2)},$$

where $s_n^o(z)$ and $s_n^e(z)$ are the Chandrasekhar functions and λ_n are the roots of the appropriate characteristic equations results from $s_n(\pm 1/2) = \partial_z s_n(\pm 1/2)$ [19].

APPENDIX B: PROJECTION INTEGRALS

Poiseuille flow

Couette flow

Odd solution: $\langle ff'' \rangle = -2\pi^2(3+20\beta_a+3\pi^2\beta_a^2)/3$, $\langle f^2 \rangle = (3+32\beta_a+12\pi^2\beta_a^2)/6$, $\langle gg'' \rangle = -2\pi^2(3+20\beta_p+3\pi^2\beta_p^2)/3$, $\langle g^2 \rangle = (3+32\beta_p+12\pi^2\beta_p^2)/6$, $\langle fsg \rangle = [3+16(\beta_a+\beta_p)+12\pi^2\beta_a\beta_p]/6$, $\langle sf \rangle = \langle g \rangle = 0$, $\langle usg \rangle = (3+16\beta_p)/6$, $\langle fu \rangle = (3+16\beta_a)/6$, $\langle gw'' \rangle = -27.257-32.441\beta_p$, $\langle gw \rangle = 0.69043+3.2870\beta_p$, $\langle w[sf]'' \rangle = -27.257-32.441\beta_a$, $\langle wsf \rangle = 0.69043+3.2870\beta_a$, $\langle uu'' \rangle = -2\pi^2$, $\langle u^2 \rangle = 1/2$, $\langle ww^{(4)} \rangle = 3803.5$, $\langle ww'' \rangle = -46.050$, $\langle w^2 \rangle = 1$.

Even solution: $\langle ff'' \rangle = -\pi^2(1+4\beta_a)/2$, $\langle f^2 \rangle = (1+8\beta_a+2\pi^2\beta_a^2)/2$, $\langle gg'' \rangle = -\pi^2(1+4\beta_p)/2$, $\langle g^2 \rangle = (1+8\beta_p+2\pi^2\beta_p^2)/2$, $\langle fsg \rangle = [1+4(\beta_a+\beta_p)+2\pi^2\beta_a\beta_p]/2$, $\langle sf \rangle = (2+\pi^2\beta_a)/\pi$, $\langle g \rangle = (2+\pi^2\beta_p)/\pi$, $\langle usg \rangle = (1+4\beta_p)/2$, $\langle fu \rangle = (1+4\beta_a)/2$, $\langle gw'' \rangle = -6.8828$, $\langle gw \rangle = 0.69738+2.6102\beta_p$, $\langle w[sf]'' \rangle = -6.8828$, $\langle wsf \rangle = 0.69738+2.6102\beta_a$, $\langle uu'' \rangle = -\pi^2/2$, $\langle u^2 \rangle = 1/2$, $\langle ww^{(4)} \rangle = 500.56$, $\langle ww'' \rangle = -12.303$, $\langle w^2 \rangle = 1$.

Odd solution: $\langle ff'' \rangle = -2\pi^2(3+20\beta_a+3\pi^2\beta_a^2)/3$, $\langle f^2 \rangle = (3+32\beta_a+12\pi^2\beta_a^2)/6$, $\langle gg'' \rangle = -\pi^2(1+4\beta_p)/2$, $\langle g^2 \rangle = (1+8\beta_p+2\pi^2\beta_p^2)/2$, $\langle fsg \rangle = -[16+9\pi^2(\beta_a+\beta_p)+72\pi^2\beta_a\beta_p]/(18\pi^2)$, $\langle sf \rangle = -(1+8\beta_a)/(2\pi)$, $\langle g \rangle = (2+\pi^2\beta_p)/\pi$, $\langle usg \rangle = -(16+9\pi^2\beta_p)/(18\pi^2)$, $\langle fu \rangle = (3+16\beta_a)/6$, $\langle gw'' \rangle = -6.8828$, $\langle gw \rangle = 0.69738+2.6102\beta_p$, $\langle w[sf]'' \rangle = -0.87673-22.615\beta_a$, $\langle wsf \rangle = -0.10292-0.49816\beta_a$, $\langle uu'' \rangle = -2\pi^2$, $\langle u^2 \rangle = 1/2$, $\langle ww^{(4)} \rangle = 500.56$, $\langle ww'' \rangle = -12.303$, $\langle w^2 \rangle = 1$.

Even solution: $\langle ff'' \rangle = -\pi^2(1+4\beta_a)/2$, $\langle f^2 \rangle = (1+8\beta_a+2\pi^2\beta_a^2)/2$, $\langle gg'' \rangle = -2\pi^2(3+20\beta_p+3\pi^2\beta_p^2)/3$, $\langle g^2 \rangle = (3+32\beta_p+12\pi^2\beta_p^2)/6$, $\langle fsg \rangle = -[16+9\pi^2(\beta_a+\beta_p)+72\pi^2\beta_a\beta_p]/(18\pi^2)$, $\langle sf \rangle = \langle g \rangle = 0$, $\langle usg \rangle = -(16+9\pi^2\beta_p)/(18\pi^2)$, $\langle fu \rangle = (1+4\beta_a)/2$, $\langle gw'' \rangle = -27.257-32.441\beta_p$, $\langle gw \rangle = 0.69043+3.2870\beta_p$, $\langle w[sf]'' \rangle = 4.4917$, $\langle wsf \rangle = -0.12206-0.59694\beta_a$, $\langle uu'' \rangle = -\pi^2/2$, $\langle u^2 \rangle = 1/2$, $\langle ww^{(4)} \rangle = 3803.5$, $\langle ww'' \rangle = -46.050$, $\langle w^2 \rangle = 1$.

-
- [1] P. Pieranski and E. Guyon, *Solid State Commun.* **13**, 435 (1973).
 [2] P. Pieranski and E. Guyon, *Phys. Rev. A* **9**, 404 (1974).
 [3] E. Dubois-Violette and P. Manneville, in *Pattern Formation in Liquid Crystals*, edited by A. Buka and L. Kramer (Springer-Verlag, New York, 1996), Chap. 4, p. 91.
 [4] P. Manneville, *J. Phys. (Paris)* **40**, 713 (1979).
 [5] P. Pieranski and E. Guyon, *Commun. Phys. (London)* **1**, 45 (1976).
 [6] P. E. Cladis and S. Torza, *Phys. Rev. Lett.* **35**, 1283 (1975).
 [7] P. J. Kedney and F. M. Leslie, *Liq. Cryst.* **24**, 613 (1998).
 [8] I. Sh. Nasibullayev, A. P. Krekhov, and M. V. Khazimullin, *Mol. Cryst. Liq. Cryst. Sci. Technol., Sect. A* **351**, 395 (2000).
 [9] O. S. Tarasov, A. P. Krekhov, and L. Kramer, *Liq. Cryst.* **28**, 833 (2001).
 [10] I. Sh. Nasibullayev and A. P. Krekhov, *Crystallogr. Rep.* **46**, 488 (2001).
 [11] O. S. Tarasov, *Liq. Cryst.* **31**, 1235 (2004).
 [12] V. G. Chigrinov, *Liquid Crystal Devices: Physics and Applications* (Artech House, New York, 1999).
 [13] P. G. de Gennes and J. Prost, *The Physics of Liquid Crystals* (Clarendon Press, Oxford, 1993).
 [14] Elastic constants in units 10^{-12} N: $K_{11}=6.66$, $K_{22}=4.2$, $K_{33}=8.61$; viscosity coefficients in units 10^{-3} Pa s: $\alpha_1=-18.1$, $\alpha_2=-110.4$, $\alpha_3=-1.1$, $\alpha_4=82.6$, $\alpha_5=77.9$, $\alpha_6=-33.6$.
 [15] P. Manneville and E. Dubois-Violette, *J. Phys. (Paris)* **37**, 285 (1976).
 [16] F. M. Leslie, *Mol. Cryst. Liq. Cryst.* **37**, 335 (1976).
 [17] E. Guyon and P. Pieranski, *J. Phys. (Paris), Colloq.* **36**, C1-203 (1975).
 [18] I. Janossy, P. Pieranski, and E. Guyon, *J. Phys. (Paris)* **37**, 1105 (1976).
 [19] S. Chandrasekhar, *Hydrodynamic and Hydromagnetic Stability* (Oxford University Press, New York, 1961).